Isoreticular Three-Dimensional Kagome Metal-Organic Frameworks with Open-Nitrogen-Donor Pillars for Selective Gas Adsorption

Andy Dinh,[†] *Huajun Yang,* [†] *Fang Peng,* [†] *Tony C. Nguyen,* [†] *Anh Hong,* [‡] *Pingyun Feng,* [‡] *and Xianhui Bu*[*,†]

[†] Department of Chemistry and Biochemistry, California State University, Long Beach, California 90840, United States.

[‡] Department of Chemistry, University of California, Riverside, California 92521, United States.

ABSTRACT

Here, we report a double-bent-ligand strategy which addresses a commonly encountered challenge in the construction of pillar-layered structures with corrugated layers which are common for non-linearly coordinated ligands and low-symmetry chiral ligands. Specifically, we show here that out-of-alignment metal coordination sites between two adjacent and opposing layers caused by in-layer bent-type ligands could be joined by another ligand type with a matching bent angle. Two isoreticular metal-organic frameworks, CPM-63m and CPM-63a, are presented here to illustrate

the implementation of this strategy. Specifically, [$Zn_2(RCOO)_4$] paddlewheel dimers are bridged by bent FDC^{2-} (H_2FDC=2,5-furandicarboxylic acid) to form neutral Kagome layers. The resulting corrugated layers are successfully pillared by bent MTZ^- (HMTZ=5-methyltetrazole) or ATZ^- ligands (HATZ=5-aminotetrazole). Furthermore, the MTZ^- and ATZ^- pillars offer open N-donor sites, and gas sorption studies of N_2, CO_2, CH_4, C_2H_2, C_2H_4, and C_2H_6 show these materials are highly porous. In addition, they exhibit interesting inverse ethane/ethylene separation property and good CO_2/CH_4 separation.

1. INTRODUCTION

While sophisticated ligand design has played an increasingly important role in new materials discovery processes,[1-4] the use of simple and readily available ligands continues to offer fascinating new materials types and at the same time offers deeper insight into key synthetic and structural parameters in the materials design.[5-9] Such phenomenon is especially true for metal-organic frameworks (MOFs) which have been widely investigated for many applications including gas storage,[10-13] gas separation,[14-16] catalysis,[17-19] drug delivery[20-22], and so on.[23-25] This is because compared with other crystalline porous materials (CPM), MOFs have far richer compositional and topological diversity.[26-28] For example, various functionalized and/or elongated ligands could be used to synthesize the same topologic structural

type in various types of MOFs (e.g., IRMOF-74 series),[29-31] _ENREF_25 which allow for the systematic design of both pore structure and functionality.

To create new topological types and to create isoreticular series of the same framework type in tunable chemical compositions represent two broad pathways in the MOF design.[32,33] For the synthetic design of isoreticular MOFs which is the theme of the work reported here, the tolerance of a given topological type to the variation in the structural features of the basic building blocks is of great interest. Of general interest is whether the lost tolerance caused by one structural parameter can be restored with a change in another independent structural parameter.[34] A prominent factor in this regard is the coordination orientation of ligand functional groups and the related metal nodes because a small difference could lead to a completely different topology or no crystallization at all.[35] In general, it is hard to replicate network topology of linear-ligand-based MOFs with bent ligands, especially those having high bent angles. This is particularly true for a MOF system with only one type of ligand. An interesting example is that while MIL-88/MOF-525-type MOFs (*acs* topology) can be readily constructed with metal trimers and linear terephthalate ligand,[36,37] the combination of bent FDC^{2-} ligand and trimers has been shown to give the *pcu*-type framework.[38] This is an example of the *acs*-to-*pcu* conversion caused by the ligand bending. Intriguingly, the reverse topological conversion (the *pcu*-to-*acs* caused by the ligand bending) has recently been found with $[Zn_4O]^{6+}$ tetramers. In this case, while MOF-5-type MOFs are constructed with $[Zn_4O]^{6+}$ and linear dicarboxylic

ligand and has *pcu* topology,[39] the *acs*-type framework was obtained when $[Zn_4O]^{6+}$ tetramers are joined with a bent dicarboxylic ligand.[40] Since each ligand in the *pcu* and *acs* nets plays the identical role as far as the net type is concerned, the suppression of the *pcu-acs* transformation in either direction proves challenging. In this work, we have studied the Kagome type lattice involving two types of ligands, and we show here an example of restoring the tolerance of the Kagome lattice to bent layer-forming ligands with matching bent layer-pillaring ligands.

Parallel to the afore-mentioned two well-known topological types for trimer- and tetramer-based materials (cubic *pcu* or hexagonal *acs* nets) whose formation is much affected by the ligand bent angles, there are also two well-known structural patterns formed from paddlewheel dimers. In fact, a recurring structural mode for paddlewheel dimers such as $[Zn_2(RCOO)_4]$ is the formation of the 2-D layers with one ligand type and the pillaring of layers with another type of ligand. In general, the 2-D layer is of the square net type with all 4-membered rings when either bent or linear ligands are used.[41,42] In comparison, the 2-D Kagome lattice based on the two different ring sizes of 3 and 6 (denoted kgm) has been much infrequently observed.[43] It has been reported that three-dimensional Kagome lattice (denoted kag) could be constructed with Kagome layers made from paddlewheel building unit bridged with linear dicarboxylic ligand, and further pillared by linear N-donor ligand.[44] However, no kag lattice based on bent ligands has been reported even though kgm layers have been found to occur

with paddlewheel unit and bent dicarboxylate including FDC^{2-} and m-BDC^{2-} (H_2m-BDC= isophthalic acid).[45]

A key issue related to the formation of paddlewheel-based pillar-layered lattice is the alignment of dimer axial sites pointing towards the interlayer region. For linear dicarboxylate, they are aligned 180°, which matches well with common linear N-donor ligands. When a bent dicarboxylate is used, the alignment of dimer axial sites deviates greatly from 180° and usually varies according to the ligand type (e.g., H_2FDC, H_2m-BDC, thiophenedicarboxylic acid, D-camphoric acid, and L-isocamphoric acid).[46] Because of such variations in the ligand-dependent alignment of axial coordination sites, finding a matching bent pillaring ligand is far less straightforward that the construction of materials based in linear ligands.

To target the synthesis of three-dimensional Kagome lattice with bent dicarboxylates, herein, we propose a 'double-bent' strategy with CPM-63m and CPM-63a as illustrative examples. This strategy involves the use of another bent N-donor ligand (Scheme 1). Compared with the linear pillar, the binding angle towards two adjacent layers offered by the bent ligands chosen in this work matches well with non-linearly oriented axial binding sites of paddlewheels in adjacent layers, which leads to successful pillaring of the corrugated layers. Interestingly, the tetrazolate pillars offer two or more open N-donor sites and the resulting material show good CO_2/CH_4 separation property and inversed ethane/ethylene separation.

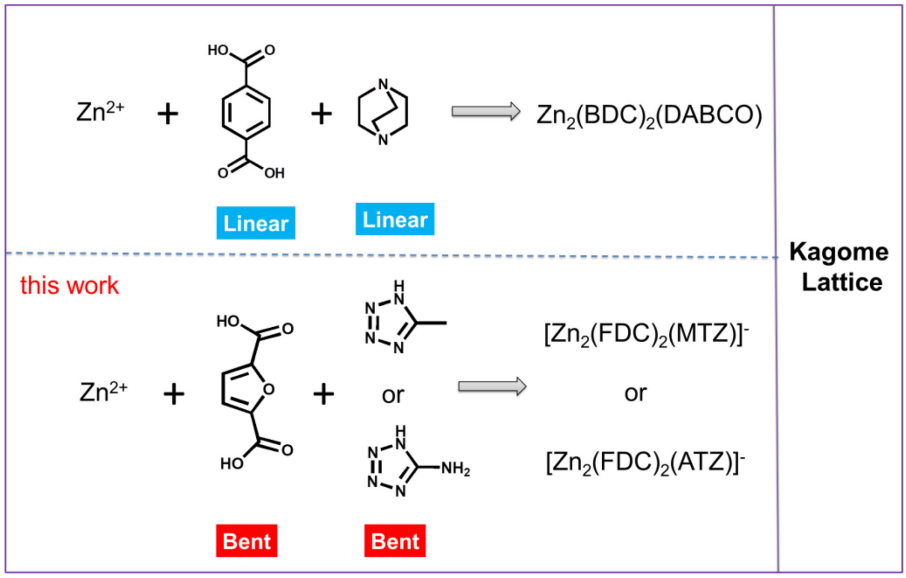

Scheme 1. Comparison of building scheme in CPM-63m and CPM-63a with $Zn_2(BDC)_2(DABCO)$ for three-dimensional Kagome lattice. Note that DABCO can also be replaced by linear 4,4-bipyridine.

2. EXPERIMENTAL SECTION

Chemicals and Materials. All chemicals were all used as supplied without any further purification.

Synthesis of CPM-63m ($[Zn_2(FDC)_2(MTZ)][(CH_3)_2NH_2]$) (CCDC No. 1985727): A mixture of $Zn(CH_3COO)_2{\cdot}2H_2O$ (44.1 mg, 0.201 mmol), 5-Methyl-1H-Tetrazole (HMTZ) (8.7 mg, 0.103 mmol), 2,5-furandicarboxylic acid (H_2FDC) (31.7 mg, 0.203 mmol), and N,N-dimethylformamide (DMF) (5 mL) was added to a 25 mL glass vial and stirred for 30 minutes. The glass vial was sealed and heated in a 120 °C oven for

five days. After 5 days, the vial was removed from the oven and allowed to naturally cool to room temperature. Clear crystals were collected and washed with DMF. The yield is calculated to be 58% based on the amount of Zn used.

Synthesis of CPM-63a ($[Zn_2(FDC)_2(ATZ)]^{-}\cdot[(CH_3)_2NH_2]^{+}$) (CCDC No. 1985726): A mixture of $Zn(CH_3COO)_2\cdot 2H_2O$ (43.7 mg, 0.199 mmol), 5-Amino-1H-Tetrazole (HATZ) (8.5 mg, 0.100 mmol), 2,5-furandicarboxylic acid (H_2FDC) (31.0 mg, 0.199 mmol), and N,N-dimethylformamide (DMF) (5 mL) was added to a 25 mL glass vial and stirred for 30 minutes. The glass vial was sealed and heated in a 120 ℃ oven for five days. After 5 days, the vial was removed from the oven and allowed to naturally cool to room temperature. Clear crystals were collected and washed with DMF. The yield is calculated to be 63% based on the amount of Zn used.

Single-Crystal X-ray Diffraction Characterization. Single-crystal X-ray diffraction was performed on a Bruker Smart APEX II CCD area diffractometer at room temperature using graphite-monochromated MoKα (λ= 0.71073 Å) radiation, operating in the ω and φ scan mode. Diffraction data was integrated and scaled by 'multi-scan' method with the Bruker APEX software. The structure was solved with the SHELXTL package and Olex2 program using intrinsic phasing method and refined with least squares analysis. All non-hydrogen atoms were refined with anisotropically. The residual electron peaks inside the lattice pores from the solvents

and cations could not be modelled and were removed using the Squeeze function from PLATON software.

Powder X-ray Diffraction (PXRD) Characterization. Powder X-ray diffraction experiments were performed on a PANalytical X'Pert Pro MPD diffractometer, equipped with a linear X'Celerator detector operating at 40 kV and 35 mA (Cu Kα radiation, λ = 1.5418 Å). The data collection was performed at room temperature in the range from 5° to 40° with a step size of ~0.008°.

Thermogravimetric (TG) Measurement. A TA Instruments TGA Q500 thermal analyzer was used to measure the TG curve by heating the sample from 30 ℃ to 800 ℃ with heating rate of 5 ℃/min under nitrogen flow. The flow rate of the nitrogen gas was controlled at about 60 milliliters per minute.

Gas Sorption Measurement. Gas sorption measurements were carried out on a Micromeritics ASAP 2020 PLUS Physisorption Analyzer. The as-synthesized sample was first allowed to cool to room temperature and then washed with DMF. The sample was then activated by solvent exchange in dichloromethane for 3 days, with the solution being refreshed every 24 hours. The dichloromethane was decanted then the sample was dried under air flow. Before gas adsorption, the sample was degassed using the degas function of the analyzer at 60 ℃ for 12 hours. N_2 adsorption was measured at 77 K. CO_2, CH_4, C_2H_2, C_2H_4, and C_2H_6 adsorption isotherms were measured at both 273 K and 296 K.

Isosteric Heat of Adsorption (Q_{st}). The isosteric heats of adsorption for CO_2, CH_4, C_2H_2, C_2H_4, and C_2H_6 were calculated using the isotherms at 273 K and 298 K, following the Clausius-Clapeyron equation with the program embedded in the software of ASAP 2020 plus. High accuracy of the Q_{st} was found in all the calculations as evidenced by the linearity in the isosters.

Selectivity by IAST. To evaluate CO_2/CH_4 and C_2H_6/C_2H_4 separation performance, the selectivities were calculated by ideal adsorbed solution theory (IAST). Single-site or dual-sites Langmuir-Freundlich (SLF or DLF) model was employed to fit the gas adsorption isotherms over the entire pressure range. SLF model can be written as:

$$N = \frac{N_{sat} b p^{1/n}}{1 + b p^{1/n}} \tag{1}$$

DLF model can be written as:

$$N = N_1 + N_2 = \frac{N_{1,sat} b_1 p^{1/n_1}}{1 + b_1 p^{1/n_1}} + \frac{N_{2,sat} b_2 p^{1/n_2}}{1 + b_2 p^{1/n_2}} \tag{2}$$

where N is the quantity adsorbed, p is the pressure of bulk gas at equilibrium with adsorbed phase, N_{sat} is the saturation loadings for adsorption site, and b are the affinity parameters. 1/n is the index of heterogeneity. The R factors for all the fitting are higher than 99.9%.

The detailed methodology for calculating the amount of A and B adsorption from a mixture by IAST is described elsewhere.[47] The adsorption selectivity is finally defined as:

$$\text{Selectivity} = \frac{q_A/q_B}{p_A/p_B} \tag{3}$$

where q_i (i = A or B) is the uptake quantity in the mixture and p_i is the feeding partial pressure of component i.

3. RESULTS AND DISCUSSIONS

Bent Kagome Lattice and Layer-Pillar Binding-Angle Match A key structural feature is the formation of 2-D Kagome lattice when Zn_2 paddlewheels are connected by 2-connected bent FDC^{2-} crosslinkers. CPM-63m crystalizes in a hexagonal system with the space group *P6₃/mmc*. It has a formula of $[Zn_2(MTZ)(FDC)_2]^-$ $[(CH_3)_2NH_2]^+$. The building block of CPM-63m is the Zn_2 paddlewheel, which is formed when two Zn atoms are held together by the coordination of 4 carboxylate groups from four FDC^{2-} ligands (Schemes S1). Each paddlewheel connects with four adjacent paddlewheels with FDC^{2-} ligand as the bridge, forming a two-dimensional Kagome net with trigonal and hexagonal pores (Figure 1a). The length between adjacent dimers (from dimer center to center) is

measured to be 9.58 Å (Figure S2). CPM-63a is isostructrual to CPM-63m except that the MTZ^- is replaced by ATZ^-.

Unlikely commonly observed pillar-layered structures, the orientation of the open metal sites from the paddlewheel is not perpendicular to the Zn_2-FDC layer due to the bent configuration of FDC^{2-}. It should also be noted that, unlike the flexible square layer, the 3-ring-containing Kagome layer is quite rigid, which limits the range of the geometric conformation of the $[Zn_2(RCOO)_4]$ paddlewheels and the orientation of axial open metal sites. As such, it is unlikely that the corrugated layers could be accommodative enough to be pillared by the linear N-donor ligand.

We reported earlier that corrugated layers made from $Zn_2(RCOO)_4$ paddlewheels and chiral D-camphorate could be pillared through the use of an X-type TPB ligand (TPB = 1,2,4,5-tetra(4-pyridyl)benzene).[46] However, the use of TPB requires both binding-angle matching (bite angle of two pyridyl groups at the left or right side of X) and the binding-site distance matching (distance between N-sites of two top or two bottom pyridyl groups in X). The flexibility of the square net made from $Zn_2(RCOO)_4$ paddlewheels and D-camphorate may have contributed to the success of the X-pillaring scheme in this earlier work.

Table 1. Crystal data and structure refinements for CPM-63m and CPM-63a

Identification code	CPM-63m	CPM-63a
Empirical formula	$C_{14}H_7N_4O_{10}Zn_2$	$C_{13}H_6N_5O_{10}Zn_2$
Formula weight	521.98	522.97
Temperature	296(2) K	296(2) K
Wavelength	0.71073 Å	0.71073 Å
Crystal system	Hexagonal	Hexagonal
Space group	$P6_3/mmc$	$P6_3/mmc$
Unit cell dimensions	a = 19.158(2) Å α= 90°. b = 19.158(2) β= 90°. c = 17.639(2) Å γ= 120°.	a = 19.049(3) Å α= 90°. b = 19.049(3) Å β= 90°. c = 17.487(3) Å γ= 120°.
Volume	5606.7(13) $Å^3$	5495(2) $Å^3$
Z	6	6
Density (calculated)	0.928 Mg/m^3	0.948 Mg/m^3
Absorption coefficient	1.315 mm^{-1}	1.343 mm^{-1}
F(000)	1554	1554
Theta range for data collection	1.685 to 25.378°	1.697 to 25.087°
Index ranges	-18<=h<=22, -23<=k<=17, -21<=l<=21	-22<=h<=22, -22<=k<=22, -20<=l<=20
Reflections collected	35642	33206
Independent reflections	1957 [R(int) = 0.1068]	1854 [R(int) = 0.0750]
Completeness to theta = 25.242°	99.9 %	99.5 %
Refinement method	Full-matrix least-squares on F^2	Full-matrix least-squares on F^2
Data / restraints / parameters	1957 / 0 / 78	1854 / 54 / 78
Goodness-of-fit on F^2	1.075	1.076
Final R indices [I>2σ(I)]	R_1 = 0.0387, wR_2 = 0.0922	R_1 = 0.0558, wR_2 = 0.1683
R indices (all data)	R_1 = 0.0719, wR_2 = 0.1064	R_1 = 0.0898, wR_2 = 0.2021
Largest diff. peak and hole	0.332 and -0.316 $e.Å^{-3}$	0.956 and -1.250 $e.Å^{-3}$

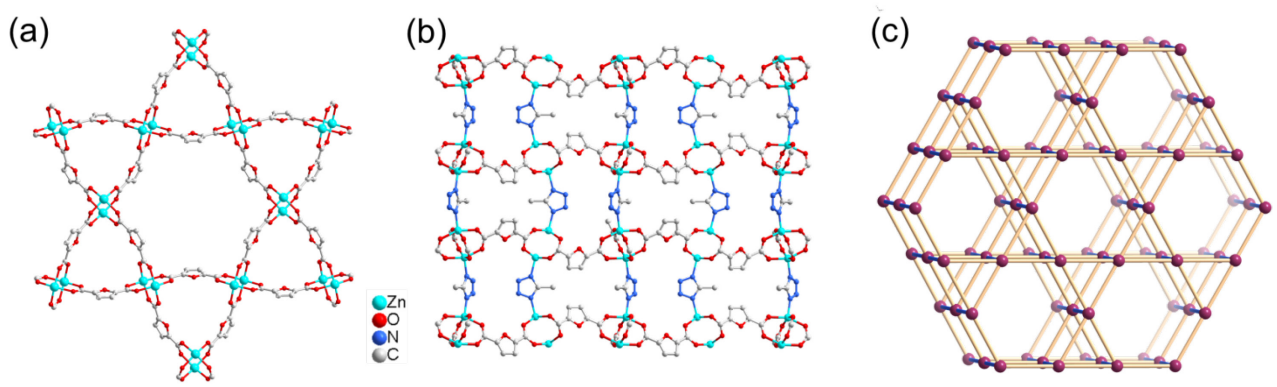

Figure 1. Structural illustration of CPM-63m: (a) The Kagome layer formed by Zn_2 paddlewheel and FDC^{2-}; (b) the Kagome layers are further pillared by MTZ^{-}; (c) the simplified kag net with purple ball representing the Zn_2 paddlewheel.

For less flexible Kagome lattice, in this work, we illustrate and highlight an alternative double-bent strategy which does not require the binding-site distance matching. Given the intrinsic capacity to form corrugated Zn_2-FDC layers, we systematically studied a series of bent ligands (e.g., imidazoles, triazoles, and tetrazoles) and found that tetrazole ligands could serve our purpose of pillaring the corrugated Kagome layers (Figure 1b). Since the binding angles for these azolate ligands are all similar, the success with tetrazolates as pillars is likely because the acidity of tetrazoles (pK_a = 4.9 for tetrazole) is much closer to H_2FDC ligand (pK_a = 2.28), than those of imidazoles and triazoles (pK_a = 14.5 and 9.97 for imidazole and 1,2,4-triazole, respectively). In the structure, the bent angle of FDC^{2-} was found to be 136.6° (a deviation of 43.4° from linear configuration) (Figure S2). By treating the

Zn_2 paddlewheel as node, the topology can be simplified as *kag* (i.e., three-dimensional Kagome structure) (Figures 1c and 2). It should be noted that this is likely the first case that the three-dimensional linear BDC-based structural type is replicated by a highly bent FDC ligand.

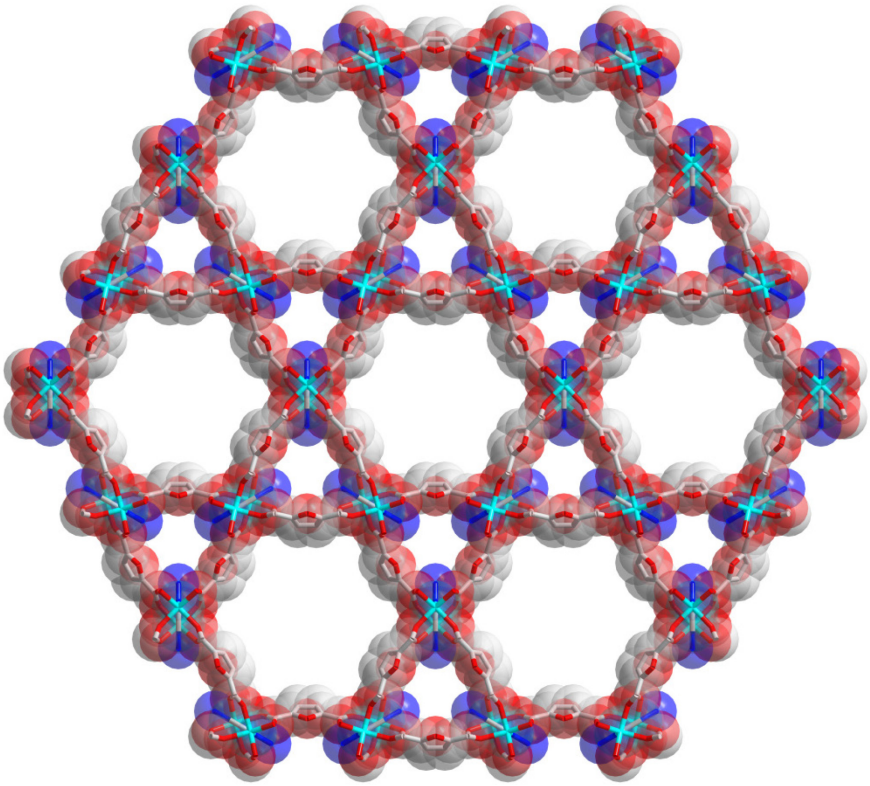

Figure 2. A perspective view of CPM-63m along the *c* axis in space-filling mode.

Another novel structural feature of CPM-63m and CPM-63a is that the ligand charge combination is -2/-1 rather than -2/0 commonly found for pillared MOF structures.[41] In the previous structures, the neutral Kagome layer is pillared by neutral pyridine ligands, resulting in a neutral framework. In contrast, in CPM-63m and

CPM-63a, the neutral layer is pillared by negative tetrazolate ligand, rending the whole framework negative. The charge of the negative framework is believed to be balanced by dimethylammonium cation, $(CH_3)_2NH_2^+$ coming from the decomposition of DMF.

Stability, Porosity, and Gas Uptake and Separation Properties The purity of the sample was verified by comparing the samples' powder X-ray patterns with simulated ones generated from the single-crystal data (Figure S3). TGA analysis indicated a high thermal decomposition temperature of 350 °C (Figure S4). The guest-accessible volume of CPM-63m is determined to be 61.4%, by the PLATON program. The actual accessible volume is lower due to the existence of the charge-balanced species within the pores.

Gas sorption properties for six different gasses (N_2, CO_2, CH_4, C_2H_2, C_2H_4, and C_2H_6) were studied here. The experiments show that both CPM-63m and CPM-63a are highly porous, which is impressive considering that they are made from very small ligands and that there is a significant pore-blockage effect exerted by charge-balancing cations. Nitrogen adsorption was measured at 77 K to determine the surface areas of CPM-63m and CPM-63a (Figure 3). It was found that CPM-63m and CPM-63a had a Brunauer–Emmett–Teller surface area of 1023 and 1127 cm^2/g, a Langmuir Surface Area of 1191.0 and 1296 cm^2/g, and a micropore volume of 0.388 and 0.449 cm^3/g, respectively.

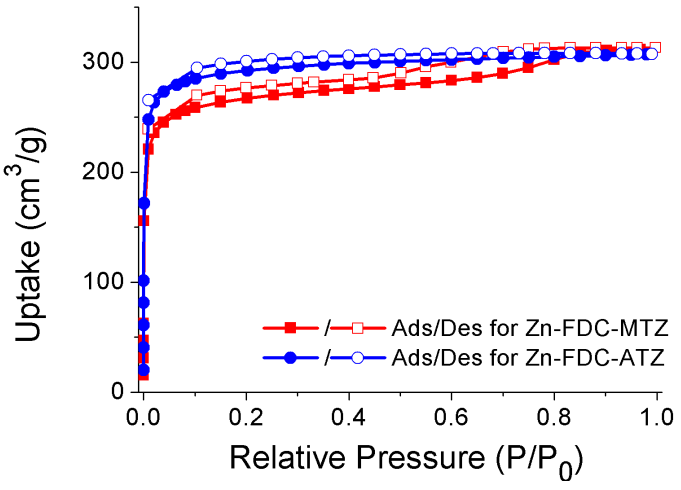

Figure 3. Nitrogen adsorption at 77 K for CPM-63m and CPM-63a.

Since MTZ^- and ATZ^- only use two nitrogen atoms to connect with inorganic nodes, open N-donor sites are available as potential gas binding sites, which could be beneficial for gas separation purpose. Multiple gases have been studied to examine the gas storage and separation performance of CPM-63m and CPM-63a. CPM-63m and CPM-63a were found to have comparable gas adsorption properties for all the test gases (Table 2 & Figures S5-8). This is probably because that the gas adsorption sites in both structures are dominated by the two open basic N sites on the tetrazolate ring, making the influence from the substituent group negligible. As a result, CPM-63m was selected to discuss the gas adsorption properties.

Table 2. Summary of Gas adsorption performances of CPM-63m and CPM-63a

MOFs	BET	Gas uptakes at RT (cm^3/g)					Q_{st}^0 (-kJ/mol)				
	(m^2/g)	C_2H_6	C_2H_4	C_2H_2	CO_2	CH_4	C_2H_6	C_2H_4	C_2H_2	CO_2	CH_4
CPM-63m	1023	63.7	56.6	76.4	43.9	13.3	31.8	29.8	30.5	26.6	18.9
CPM-63a	1127	64.0	56.3	72.8	47.2	14.0	33.9	30.0	29.2	26.7	21.0

To probe the potential applications in CO_2/CH_4 separation, isotherms of CO_2 and CH_4 were measured at both 273 K and 298 K. CPM-63m has saturated uptakes of 78.4 cm^3/g and 43.9 cm^3/g of carbon dioxide at 273 K and 298 K, respectively. By contrast, it could only adsorb 20.0 cm^3/g and 13.3 cm^3/g of methane at 273 K and 298 K, respectively. Based on the temperature-dependent isotherms, the heat of adsorption at zero coverage was determined to be of -26.6 kJ/mol for carbon dioxide and -18.9 kJ/mol for methane, indicating a good CO_2/CH_4 separation property. A relatively high IAST selectivity of 5.1 was also obtained (Figure 4), which is higher than ZIF-68-70 (3.2-3.8),[48] NH_2-MIL-125(3.9), and activated carbon (2.3).[49]

It has been reported that materials without open-metal sites can have unique applications in the storage and separation of hydrocarbon gas molecules including C_2H_6-selective C_2H_6/C_2H_4 separation.[50] As an alternative to the recently reported 9-connected *pacs* platform, the 6-connected 3-D Kagome lattice described here represents another prototype of framework topology without open-metal sites, but capable of open-Lewis-base sites as shown here. The gas sorption measurements of acetylene, ethylene, and ethane were conducted. At 296 K, the gas sorption quantity reaches 76.4, 56.6, and 63.7 cm^3/g for acetylene, ethylene, and ethane, respectively (Figure S5). At 273 K, they increase to 126.0, 89.6, and 98.7 cm^3/g, respectively. Heat of adsorptions at near-zero coverage were determined to be 30.5, 29.8, and 31.8 kJ/mol for acetylene, ethylene, and ethane, respectively. Interestingly, the inversed ethane/ethylene separation was observed in CPM-63m. The C_2H_6/C_2H_4 selectivity are

calculated to be 1.41 at 1 bar, which is comparable to some benchmark materials including TJT-100 (1.2),[51] CPM-233 (1.64),[50] and MIL-142A (1.51).[52]

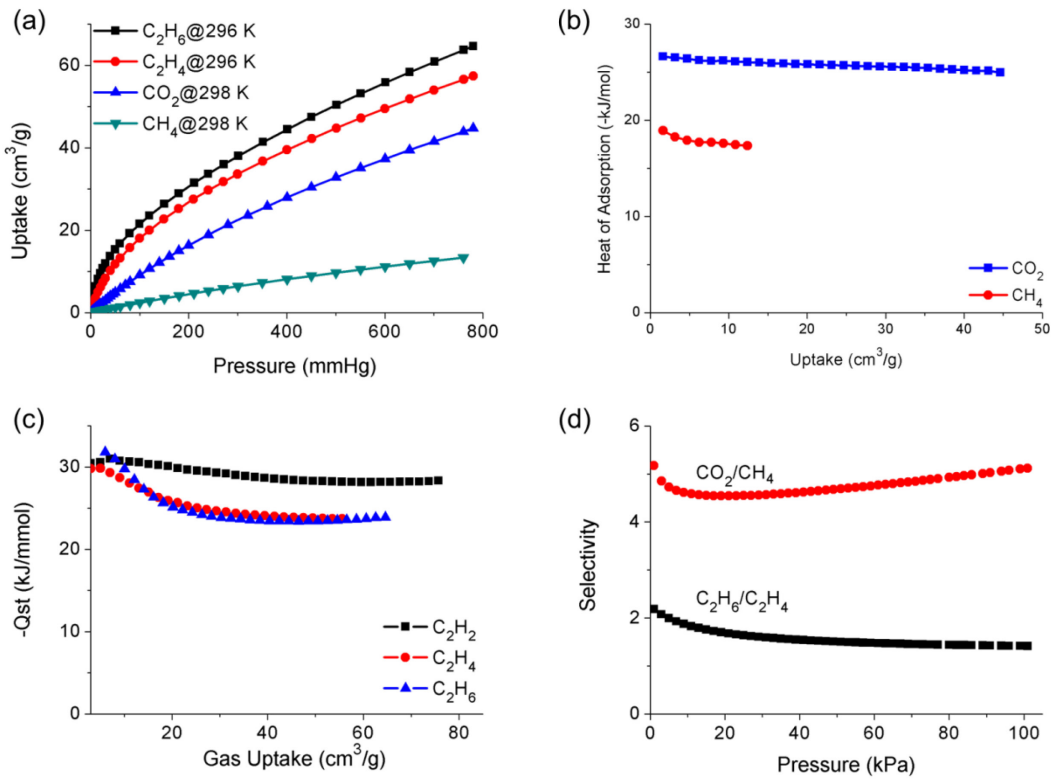

Figure 4. (a) CO_2 and CH_4 adsorption isotherms of CPM-63m at 298 K; (b) CO_2 and CH_4 adsorption enthalpy for CPM-63m; (c) C_2H_2, C_2H_4, and C_2H_6 adsorption enthalpy for CPM-63m (d) CO_2/CH_4 and C_2H_6/C_2H_4 IAST selectivity for equimolar mixture at room temperature.

4. CONCLUSION

In summary, two three-dimensional Kagome metal-organic frameworks were synthesized in this work through a double-bent route. While the synthesis of isostructures is common in metal-organic frameworks, the use of bent ligands to

replicate the structures predominantly based on linear ligands, as shown here, is far less common. The combined use of two bent ligands provides a generalized approach to create new structures with targeted topology. The 2-connected coordination mode of tetrazolates in these two structures is interesting and leaves open Lewis basic N sites and resulting materials show good CO_2/CH_4 separation property and interesting inversed C_2H_6/C_2H_4 separation.

ASSOCIATED CONTENT

Supporting Information

The Supporting Information is available free of charge at https://pubs.acs.org.

Additional structural figures, TGA curves and additional adsorption isotherms (PDF)

Accession Codes

CCDC 1985726−1985727 contain the supplementary crystallographic data for this paper. These data can be obtained free of charge via www.ccdc.cam.ac.uk/data_request/cif, or by emailing data_request@ccdc.cam.ac.uk, or by contacting The Cambridge Crystallographic Data Centre, 12 Union Road, Cambridge CB2 1EZ, UK; fax: +44 1223 336033.

AUTHOR INFORMATION

Corresponding Author

E-mail: xianhui.bu@csulb.edu

Notes

The authors declare no competing financial interest.

ACKNOWLEDGMENT

We thank the support by NSF-DMR, under award NO. 1708850 (X.B.) and CSULB RSCA award (X.B.).

REFERENCES

(1) Furukawa, H.; Ko, N.; Go, Y. B.; Aratani, N.; Choi, S. B.; Choi, E.; Yazaydin, A. Ö.; Snurr, R. Q.; O'Keeffe, M.; Kim, J.; Yaghi, O. M. Ultrahigh Porosity in Metal-Organic Frameworks. *Science* **2010**, *329*, 424-428.

(2) Farha, O. K.; Özgür Yazaydın, A.; Eryazici, I.; Malliakas, C. D.; Hauser, B. G.; Kanatzidis, M. G.; Nguyen, S. T.; Snurr, R. Q.; Hupp, J. T. De novo synthesis of a metal–organic framework material featuring ultrahigh surface area and gas storage capacities. *Nat. Chem.* **2010**, *2*, 944-948.

(3) Guillerm, V.; Weseliński, Ł. J.; Belmabkhout, Y.; Cairns, A. J.; D'Elia, V.; Wojtas, Ł.; Adil, K.; Eddaoudi, M. Discovery and introduction of a (3,18)-connected net as an ideal blueprint for the design of metal–organic frameworks. *Nat. Chem.* **2014**, *6*, 673-680.

(4) Bai, Y.; Dou, Y.; Xie, L.-H.; Rutledge, W.; Li, J.-R.; Zhou, H.-C. Zr-based metal–organic frameworks: design, synthesis, structure, and applications. *Chem. Soc. Rev.* **2016**, *45*, 2327-2367.

(5) Zhao, X.; Bu, X.; Zhai, Q.-G.; Tran, H.; Feng, P. Pore Space Partition by Symmetry-Matching Regulated Ligand Insertion and Dramatic Tuning on Carbon Dioxide Uptake. *J. Am. Chem. Soc.* **2015**, *137*, 1396-1399.

(6) Dan-Hardi, M.; Serre, C.; Frot, T.; Rozes, L.; Maurin, G.; Sanchez, C.; Férey, G. A New Photoactive Crystalline Highly Porous Titanium(IV) Dicarboxylate. *J. Am. Chem. Soc.* **2009**, *131*, 10857-10859.

(7) Zhai, Q.-G.; Bu, X.; Zhao, X.; Li, D.-S.; Feng, P. Pore Space Partition in Metal–Organic Frameworks. *Acc. Chem. Res.* **2017**, *50*, 407-417.

(8) Kang, M.; Luo, D.; Luo, X.; Chen, Z.; Lin, Z. Crystalline beryllium carboxylate frameworks with rutile-type and cubic-C_3N_4 topologies. *CrystEngComm* **2012**, *14*, 95-97.

(9) Liu, J.-H.; Lin, L.-D.; Li, X.-X.; Zhao, D.; Sun, Y.-Q.; Zheng, S.-T. A nested Cu24@Cu72-based copper‑organic polyhedral framework for selective adsorption of cationic dyes. *Chem. Commun.* **2019**, *55*, 7394-7397.

(10) Xiang, S.; Zhou, W.; Zhang, Z.; Green, M. A.; Liu, Y.; Chen, B. Open Metal Sites within Isostructural Metal–Organic Frameworks for Differential Recognition of Acetylene and Extraordinarily High Acetylene Storage Capacity at Room Temperature. *Angew. Chem. Int. Ed.* **2010**, *49*, 4615-4618.

(11) Spanopoulos, I.; Tsangarakis, C.; Klontzas, E.; Tylianakis, E.; Froudakis, G.; Adil, K.; Belmabkhout, Y.; Eddaoudi, M.; Trikalitis, P. N. Reticular Synthesis of HKUST-like tbo-MOFs with Enhanced CH_4 Storage. *J. Am. Chem. Soc.* **2016**, *138*, 1568-1574.

(12) Mason, J. A.; Oktawiec, J.; Taylor, M. K.; Hudson, M. R.; Rodriguez, J.; Bachman, J. E.; Gonzalez, M. I.; Cervellino, A.; Guagliardi, A.; Brown, C. M.; Llewellyn, P. L.; Masciocchi, N.; Long, J. R. Methane storage in flexible metal–organic frameworks with intrinsic thermal management. *Nature* **2015**, *527*, 357-361.

(13) Pang, J.; Jiang, F.; Wu, M.; Liu, C.; Su, K.; Lu, W.; Yuan, D.; Hong, M. A porous metal-organic framework with ultrahigh acetylene uptake capacity under ambient conditions. *Nat. Comm.* **2015**, *6*, 7575.

(14) Herm, Z. R.; Wiers, B. M.; Mason, J. A.; van Baten, J. M.; Hudson, M. R.; Zajdel, P.; Brown, C. M.; Masciocchi, N.; Krishna, R.; Long, J. R. Separation of Hexane Isomers in a Metal-Organic Framework with Triangular Channels. *Science* **2013**, *340*, 960-964.

(15) Lin, R.-B.; Li, L.; Zhou, H.-L.; Wu, H.; He, C.; Li, S.; Krishna, R.; Li, J.; Zhou, W.; Chen, B. Molecular sieving of ethylene from ethane using a rigid metal–organic framework. *Nat. Mater.* **2018**, *17*, 1128-1133.

(16) Wang, D.; Zhang, J.; Li, G.; Yuan, J.; Li, J.; Huo, Q.; Liu, Y. Mesoporous Hexanuclear Copper Cluster-Based Metal–Organic Framework with Highly Selective

Adsorption of Gas and Organic Dye Molecules. *ACS Appl. Mater. Inter.* **2018**, *10*, 31233-31239.

(17) Yang, Q.; Xu, Q.; Jiang, H.-L. Metal–organic frameworks meet metal nanoparticles: synergistic effect for enhanced catalysis. *Chem. Soc. Rev.* **2017**, *46*, 4774-4808.

(18) Wu, Y.-P.; Zhou, W.; Zhao, J.; Dong, W.-W.; Lan, Y.-Q.; Li, D.-S.; Sun, C.; Bu, X. Surfactant-Assisted Phase-Selective Synthesis of New Cobalt MOFs and Their Efficient Electrocatalytic Hydrogen Evolution Reaction. *Angew. Chem. Int. Ed.* **2017**, *56*, 13001-13005.

(19) Zhao, X.; Feng, J.; Liu, J.; Shi, W.; Yang, G.; Wang, G.-C.; Cheng, P. An Efficient, Visible-Light-Driven, Hydrogen Evolution Catalyst $NiS/Zn_xCd_{1-x}S$ Nanocrystal Derived from a Metal–Organic Framework. *Angew. Chem. Int. Ed.* **2018**, *57*, 9790-9794.

(20) Dong, Z.; Sun, Y.; Chu, J.; Zhang, X.; Deng, H. Multivariate Metal–Organic Frameworks for Dialing-in the Binding and Programming the Release of Drug Molecules. *J. Am. Chem. Soc.* **2017**, *139*, 14209-14216.

(21) Chen, Y.; Lykourinou, V.; Vetromile, C.; Hoang, T.; Ming, L.-J.; Larsen, R. W.; Ma, S. How Can Proteins Enter the Interior of a MOF? Investigation of Cytochrome c Translocation into a MOF Consisting of Mesoporous Cages with Microporous Windows. *J. Am. Chem. Soc.* **2012**, *134*, 13188-13191.

(22) Teplensky, M. H.; Fantham, M.; Li, P.; Wang, T. C.; Mehta, J. P.; Young, L. J.; Moghadam, P. Z.; Hupp, J. T.; Farha, O. K.; Kaminski, C. F.; Fairen-Jimenez, D. Temperature Treatment of Highly Porous Zirconium-Containing Metal–Organic Frameworks Extends Drug Delivery Release. *J. Am. Chem. Soc.* **2017**, *139*, 7522-7532.

(23) Liu, C.-S.; Li, J.; Pang, H. Metal-organic framework-based materials as an emerging platform for advanced electrochemical sensing. *Coord. Chem. Rev.* **2020**, *410*, 213222.

(24) Ma, X.; Chai, Y.; Li, P.; Wang, B. Metal–Organic Framework Films and Their Potential Applications in Environmental Pollution Control. *Acc. Chem. Res.* **2019**, *52*, 1461-1470.

(25) Wang, Y.; Yin, X.; Liu, W.; Xie, J.; Chen, J.; Silver, M. A.; Sheng, D.; Chen, L.; Diwu, J.; Liu, N.; Chai, Z.; Albrecht-Schmitt, T. E.; Wang, S. Emergence of Uranium as a Distinct Metal Center for Building Intrinsic X-ray Scintillators. *Angew. Chem. Int. Ed.* **2018**, *57*, 7883-7887.

(26) Furukawa, H.; Cordova, K. E.; O'Keeffe, M.; Yaghi, O. M. The Chemistry and Applications of Metal-Organic Frameworks. *Science* **2013**, *341*, 1230444.

(27) Furukawa, S.; Reboul, J.; Diring, S.; Sumida, K.; Kitagawa, S. Structuring of metal–organic frameworks at the mesoscopic/macroscopic scale. *Chem. Soc. Rev.* **2014**, *43*, 5700-5734.

(28) Stock, N.; Biswas, S. Synthesis of Metal-Organic Frameworks (MOFs): Routes to Various MOF Topologies, Morphologies, and Composites. *Chem. Rev.* **2012**, *112*, 933-969.

(29) Deng, H.; Grunder, S.; Cordova, K. E.; Valente, C.; Furukawa, H.; Hmadeh, M.; Gándara, F.; Whalley, A. C.; Liu, Z.; Asahina, S.; Kazumori, H.; O'Keeffe, M.; Terasaki, O.; Stoddart, J. F.; Yaghi, O. M. Large-Pore Apertures in a Series of Metal-Organic Frameworks. *Science* **2012**, *336*, 1018-1023.

(30) Devic, T.; Horcajada, P.; Serre, C.; Salles, F.; Maurin, G.; Moulin, B.; Heurtaux, D.; Clet, G.; Vimont, A.; Grenèche, J.-M.; Ouay, B. L.; Moreau, F.; Magnier, E.; Filinchuk, Y.; Marrot, J.; Lavalley, J.-C.; Daturi, M.; Férey, G. Functionalization in Flexible Porous Solids: Effects on the Pore Opening and the Host−Guest Interactions. *J. Am. Chem. Soc.* **2010**, *132*, 1127-1136.

(31) Yang, H.; Peng, F.; Dang, C.; Wang, Y.; Hu, D.; Zhao, X.; Feng, P.; Bu, X. Ligand Charge Separation To Build Highly Stable Quasi-Isomer of MOF-74-Zn. *J. Am. Chem. Soc.* **2019**, *141*, 9808-9812.

(32) Eddaoudi, M.; Kim, J.; Rosi, N.; Vodak, D.; Wachter, J.; O'Keeffe, M.; Yaghi, O. M. Systematic Design of Pore Size and Functionality in Isoreticular MOFs and Their Application in Methane Storage. *Science* **2002**, *295*, 469-472.

(33) Chen, Z.; Thiam, Z.; Shkurenko, A.; Weselinski, L. J.; Adil, K.; Jiang, H.; Alezi, D.; Assen, A. H.; O'Keeffe, M.; Eddaoudi, M. Enriching the Reticular Chemistry Repertoire with Minimal Edge-Transitive Related Nets: Access to Highly

Coordinated Metal–Organic Frameworks Based on Double Six-Membered Rings as Net-Coded Building Units. *J. Am. Chem. Soc.* **2019**, *141*, 20480-20489.

(34) Guillerm, V.; Grancha, T.; Imaz, I.; Juanhuix, J.; Maspoch, D. Zigzag Ligands for Transversal Design in Reticular Chemistry: Unveiling New Structural Opportunities for Metal–Organic Frameworks. *J. Am. Chem. Soc.* **2018**, *140*, 10153-10157.

(35) Schoedel, A.; Zaworotko, M. J. $[M_3(\mu_3\text{-}O)(O_2CR)_6]$ and related trigonal prisms: versatile molecular building blocks for crystal engineering of metal–organic material platforms. *Chem. Sci.* **2014**, *5*, 1269-1282.

(36) Horcajada, P.; Salles, F.; Wuttke, S.; Devic, T.; Heurtaux, D.; Maurin, G.; Vimont, A.; Daturi, M.; David, O.; Magnier, E.; Stock, N.; Filinchuk, Y.; Popov, D.; Riekel, C.; Férey, G.; Serre, C. How Linker's Modification Controls Swelling Properties of Highly Flexible Iron(III) Dicarboxylates MIL-88. *J. Am. Chem. Soc.* **2011**, *133*, 17839-17847.

(37) Sudik, A. C.; Côté, A. P.; Yaghi, O. M. Metal-Organic Frameworks Based on Trigonal Prismatic Building Blocks and the New "acs" Topology. *Inorg. Chem.* **2005**, *44*, 2998-3000.

(38) Zhai, Q.-G.; Bu, X.; Zhao, X.; Mao, C.; Bu, F.; Chen, X.; Feng, P. Advancing Magnesium–Organic Porous Materials through New Magnesium Cluster Chemistry. *Cryst. Growth Des.* **2016**, *16*, 1261-1267.

(39) Li, H.; Eddaoudi, M.; O'Keeffe, M.; Yaghi, O. M. Design and synthesis of an exceptionally stable and highly porous metal-organic framework. *Nature* **1999**, *402*, 276-279.

(40) Zhao, X.; Yang, H.; Nguyen, E. T.; Padilla, J.; Chen, X.; Feng, P.; Bu, X. Enabling Homochirality and Hydrothermal Stability in Zn_4O-Based Porous Crystals. *J. Am. Chem. Soc.* **2018**, *140*, 13566-13569.

(41) Dybtsev, D. N.; Chun, H.; Kim, K. Rigid and Flexible: A Highly Porous Metal–Organic Framework with Unusual Guest-Dependent Dynamic Behavior. *Angew. Chem. Int. Ed.* **2004**, *43*, 5033-5036.

(42) Bourne, S. A.; Lu, J.; Mondal, A.; Moulton, B.; Zaworotko, M. J. Self-Assembly of Nanometer-Scale Secondary Building Units into an Undulating Two-Dimensional Network with Two Types of Hydrophobic Cavity. *Angew. Chem. Int. Ed.* **2001**, *40*, 2111-2113.

(43) Chun, H.; Moon, J. Discovery, Synthesis, and Characterization of an Isomeric Coordination Polymer with Pillared Kagome Net Topology. *Inorg. Chem.* **2007**, *46*, 4371-4373.

(44) Kondo, M.; Takashima, Y.; Seo, J.; Kitagawa, S.; Furukawa, S. Control over the nucleation process determines the framework topology of porous coordination polymers. *CrystEngComm* **2010**, *12*, 2350-2353.

(45) Yang, J.; Lutz, M.; Grzech, A.; Mulder, F. M.; Dingemans, T. J. Copper-based coordination polymers from thiophene and furan dicarboxylates with high isosteric heats of hydrogen adsorption. *CrystEngComm* **2014**, *16*, 5121-5127.

(46) Nguyen, E. T.; Zhao, X.; Ta, D.; Nguyen, P.-L.; Bu, X. Comparative Study of In Situ and Presynthesized X-Pillar Ligand in Self-Assembly of Homochiral Porous Frameworks. *Cryst. Growth Des.* **2015**, *15*, 5939-5944.

(47) Myers, A. L.; Prausnitz, J. M. Thermodynamics of mixed-gas adsorption. *AlChE J.* **1965**, *11*, 121-127.

(48) Phan, A.; Doonan, C. J.; Uribe-Romo, F. J.; Knobler, C. B.; O'Keeffe, M.; Yaghi, O. M. Synthesis, Structure, and Carbon Dioxide Capture Properties of Zeolitic Imidazolate Frameworks. *Acc. Chem. Res.* **2010**, *43*, 58-67.

(49) Rada, Z. H.; Abid, H. R.; Shang, J.; He, Y.; Webley, P.; Liu, S.; Sun, H.; Wang, S. Effects of amino functionality on uptake of CO_2, CH_4 and selectivity of CO_2/CH_4 on titanium based MOFs. *Fuel* **2015**, *160*, 318-327.

(50) Yang, H.; Wang, Y.; Krishna, R.; Jia, X.; Wang, Y.; Hong, A. N.; Dang, C.; Castillo, H. E.; Bu, X.; Feng, P. Pore-Space-Partition-Enabled Exceptional Ethane Uptake and Ethane-Selective Ethane–Ethylene Separation. *J. Am. Chem. Soc.* **2020**, *142*, 2222-2227.

(51) Hao, H.-G.; Zhao, Y.-F.; Chen, D.-M.; Yu, J.-M.; Tan, K.; Ma, S.; Chabal, Y.; Zhang, Z.-M.; Dou, J.-M.; Xiao, Z.-H.; Day, G.; Zhou, H.-C.; Lu, T.-B. Simultaneous Trapping of C_2H_2 and C_2H_6 from a Ternary Mixture of $C_2H_2/C_2H_4/C_2H_6$ in a Robust

Metal–Organic Framework for the Purification of C_2H_4. *Angew. Chem. Int. Ed.* **2018**, *57*, 16067-16071.

(52) Chen, Y.; Wu, H.; Lv, D.; Shi, R.; Chen, Y.; Xia, Q.; Li, Z. Highly Adsorptive Separation of Ethane/Ethylene by An Ethane-Selective MOF MIL-142A. *Ind. Eng. Chem. Res.* **2018**, *57*, 4063-4069.

For Table of Contents Use Only

Isoreticular Three-Dimensional Kagome Metal-Organic Frameworks with Open-Nitrogen-Donor Pillars for Selective Gas Adsorption

*Andy Dinh, Huajun Yang, Fang Peng, Tony C. Nguyen, Anh Hong, Pingyun Feng, and Xianhui Bu**

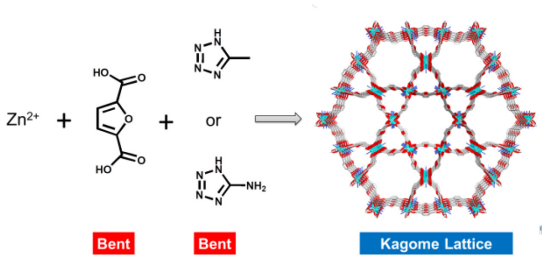

A double-bent-ligand strategy which involves the use of two bent ligands allows the construction of two isoreticular pillar-layered Kagome structures. Both structures exhibit interesting inverse ethane/ethylene separation property and good CO_2/CH_4 separation.